



Ionic conductivity of the molten systems $(\text{LiF}-\text{CaF}_2)_{\text{eut}}-\text{NdF}_3$, $(\text{LiF}-\text{NaF})_{\text{eut}}-\text{NdF}_3$, $(\text{NaF}-\text{CaF}_2)_{\text{eut}}-\text{NdF}_3$ and $(\text{LiF}-\text{MgF}_2)_{\text{eut}}-\text{NdF}_3$

Dhiya Krishnan¹ · Michal Korenko^{1,2,3} · František Šimko^{1,4} · Marta Ambrová⁵ · Lórant Szatmáry⁶ · Aydar Rakhmatullin³

Received: 24 July 2023 / Revised: 11 September 2023 / Accepted: 22 September 2023 / Published online: 11 October 2023
© The Author(s) 2023

Abstract

Experimental measurements were made to assess the electrical conductivity as a function of temperature and NdF_3 concentration (0–20 mol %) of molten systems of $(\text{LiF}-\text{CaF}_2)_{\text{eut}}-\text{NdF}_3$, $(\text{LiF}-\text{NaF})_{\text{eut}}-\text{NdF}_3$, $(\text{NaF}-\text{CaF}_2)_{\text{eut}}-\text{NdF}_3$ and $(\text{LiF}-\text{MgF}_2)_{\text{eut}}-\text{NdF}_3$. The experiment used an altering current impedance spectroscopy technique with a platinum–rhodium electrode positioned in a pyrolytic BN tube and graphite a crucible/counter electrode. The conductivity of all systems under study increased with rising temperatures and decreasing NdF_3 concentrations. The Arrhenius equation and linear regression have both been used to describe the experimental data. The results of the ionic conductivity for the temperature 850 °C and NdF_3 concentrations 0, 10 and 15 mol %, respectively, can be compared as follows: the conductivity of the molten system of $(\text{LiF}-\text{CaF}_2)_{\text{eut}}-\text{NdF}_3$ was determined to be 6.10, 5.95 and 5.10 $\text{S}\cdot\text{cm}^{-1}$, the results for the system $(\text{LiF}-\text{NaF})_{\text{eut}}-\text{NdF}_3$ were 6.16, 5.56 and 4.13 $\text{S}\cdot\text{cm}^{-1}$, the results for the system $(\text{NaF}-\text{CaF}_2)_{\text{eut}}-\text{NdF}_3$ were 3.78, 3.56 and 2.32 $\text{S}\cdot\text{cm}^{-1}$, and finally, the results for the system $(\text{LiF}-\text{MgF}_2)_{\text{eut}}-\text{NdF}_3$ were determined to be for the same temperature as 5.35, 4.79 and 4.14 $\text{S}\cdot\text{cm}^{-1}$, respectively.

Keywords Electrical/ionic conductivity · Molten salts electrolysis · Rare earth elements (REEs) · Neodymium · Molten salt reactor · Electrometallurgy

Introduction

High-temperature inorganic molten salts are attractive coulombic liquids (containing ionic components), and they are being used in many areas of industry, e.g., electrometallurgy and electrochemical recycling of metals, renewable energy technologies and up to the new class of nuclear reactors, molten salt nuclear reactors (MSR), where, in the ultimate design, the molten salt works as the liquid in the primary circuit (with the fissile/fertile material dissolved in the melt) as well as cooling medium in the heat transfer interface (secondary circuit of the reactor). Molten fluoride systems are being also seriously considered as tritium breeding blankets in nuclear fusion technology [1–11].

The knowledge of the physico-chemical performance, electrochemical characterization and structural characterization of the related molten fluorides are thus vital for the commercialization of the MSR technology. Due to the inherent features of nuclear chain reaction, rare earth elements (REEs) are being formed and present in all nuclear reactors. Insofar as their formation is concerned, they serve as neutron

✉ Michal Korenko
uachmiko@savba.sk

✉ František Šimko
uachsim@savba.sk

¹ Institute of Inorganic Chemistry, Slovak Academy of Sciences, Dúbravská Cesta 9, 845 36 Bratislava, Slovakia

² Loire Valley Institute for Advanced Studies, 1 Rue Dupanloup, 45000 Orléans, France

³ CEMHTI–Conditions Extrêmes Et Matériaux: Haute Température Et Irradiation UPR3079–(CNRS), 1D Av. de La Recherche Scientifique CS 90055, 45071 Orléans, France

⁴ Centre of Excellence for Advanced Materials Application–CEMEA, Slovak Academy of Sciences, Dúbravská Cesta 5807/9, 845 11 Bratislava, Slovakia

⁵ Faculty of Chemical and Food Technology, Slovak University of Technology in Bratislava, Radlinského 9, 812 37 Bratislava, Slovakia

⁶ Fuel Cycle Chemistry Department, ÚJV Řež a.S., 250 68 Husinec Řež, Czech Republic

poison for the nuclear process. Therefore, a solution must be developed to keep them apart from the nuclear reactor's fuel. Because in MSR technology the fuel in the primary circuit is dissolved in molten salt, this separation unit might be feasible online within the circuit. A high-temperature reprocessing based on the electrolytic separation can be thus done within the framework of MSR technology. Although this appealing concept is still being worked on, it is far simpler and more straightforward than any other fuel recycling technology [12].

Any industrial process based on molten salts can only be modeled, optimized and operated with an understanding of how the physico-chemical characteristics (ionic conductivity, density viscosity, etc.) are linked to the structure of the electrolyte. Electrical conductivity is one of the most important physico-chemical properties in electrometallurgy and other industrial electrochemical processes. This physico-chemical parameter is connected to other transport characteristics such as viscosity, diffusivity and ion mobility. The electrolyte's electrical conductivity is also correlated with the electrolysis' energy efficiency and current efficiency [13, 14]. The ionic content and the structure of the molten electrolyte impact the electrical conductivity, which can be utilized for verifying the possible formation of polymers or complex species in the melt.

The fact that the molten salt electrolyte works also as a heating element in which the Joule heat is generated owing to ohmic drop is another significant aspect of the electrical conductivity of molten systems in electrochemical separation technologies (and generally in electrometallurgy). Because of the importance of maintaining the electroseparation unit's ideal heat balance, electrical conductivity is a crucial piece of data for process design and optimization.

The topic of the present study is the experimental investigation of the high-temperature ionic electrical conductivity as a function of temperature and the concentration of NdF_3 (0–20 mol %) of the following ternary molten systems: $(\text{LiF}-\text{CaF}_2)_{\text{eut}}-\text{NdF}_3$, $(\text{LiF}-\text{NaF})_{\text{eut}}-\text{NdF}_3$, $(\text{NaF}-\text{CaF}_2)_{\text{eut}}-\text{NdF}_3$ and $(\text{LiF}-\text{MgF}_2)_{\text{eut}}-\text{NdF}_3$.

Only a few articles [15–24] briefly explore the physico-chemical properties of molten ternary systems based on LiF, NaF, CaF_2 , MgF_2 and NdF_3 . A thermal analysis of the phase equilibria and an investigation of the volume properties of the system $(\text{LiF}-\text{CaF}_2)_{\text{eut}}-\text{NdF}_3$ are both included in the work by Mlynáriková et al. [15]. A section of the phase diagram for the system $(\text{LiF}-\text{CaF}_2)_{\text{eut}}-\text{NdF}_3$ is shown in this paper. One eutectic point with the approximate coordinates of 692 °C, 20 mol % NdF_3 and a solid solution exist in this section of the phase diagram.

The works [16, 17] contain the phase equilibria study (DTA and XRD) for the system $\text{NaF}-\text{LiF}-\text{NdF}_3$. These publications claim that the system $\text{NaF}-\text{LiF}-\text{NdF}_3$ contains three invariant points, two

of which are peritectic and one of which is eutectic. The eutectic point is described by the following coordinates: composition (mol %): $\text{NaF}(33.0)-\text{LiF}(53.0)-\text{NdF}_3(14.0)$, and eutectic temperature: 580 °C. The peritectic temperatures of two peritectic points with the molar compositions $\text{NaF}(41.0)-\text{LiF}(44.0)-\text{NdF}_3(15.0)$ and $\text{NaF}(39.0)-\text{LiF}(45.0)-\text{NdF}_3(16.0)$ are 595 °C and 610 °C, respectively. NaNdF_4 is formed at the first peritectic point, which has a peritectic temperature of 595 °C, while $\text{Na}_5\text{Nd}_9\text{F}_{32}$ is formed at the second peritectic point, which has a peritectic temperature of 610 °C [16].

In the experimental work of Kubíková et al. [23], phase equilibrium and the density of the molten $(\text{LiF}-\text{MgF}_2)_{\text{eut}}-\text{NdF}_3$ system are described. Based on that research, six phase fields make up the $(\text{LiF}-\text{MgF}_2)_{\text{eut}}-\text{NdF}_3$ system's phase diagram. In the concentration range of $0 < x(\text{MgF}_2) < 0.15$, an MgF_2 -based solid solution with dissolved LiF is the primary solid. The phase field upon further cooling consists of the LiF-based solid solution with dissolved MgF_2 ($0 < x(\text{MgF}_2) < 0.10$). The MgF_2 -rich side of the phase diagram (concentration range $0.10 < x(\text{MgF}_2) < 0.30$) contains the field with NdF_3 as the only solid phase and the field with MgF_2 -based solid solution crystallizing at 777 °C. The coordinates of the ternary eutectic point are in this phase diagram 10 mol % of NdF_3 and 678 °C [23].

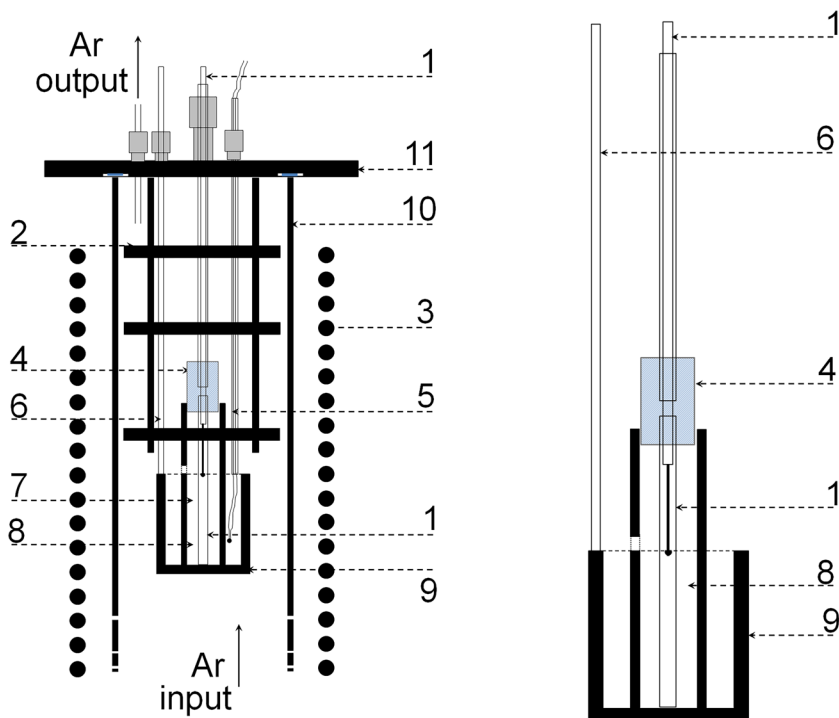
The works [18–22] contain details on the phase equilibria in the binary systems $\text{LiF}-\text{NdF}_3$, $\text{NaF}-\text{NdF}_3$ and $\text{CaF}_2-\text{NdF}_3$. The work [25] contains the high-temperature electrical conductivity analysis of the binary system $\text{LiF}-\text{NdF}_3$ (within temperature interval 950–1150 °C). The electrical conductivity of the system $\text{LiF}-\text{NdF}_3$ is in this work reported as an isothermal drop (950 °C) from 8.53 $\text{S}\cdot\text{cm}^{-1}$ for 5 mol % of NdF_3 to 5.11 $\text{S}\cdot\text{cm}^{-1}$ for 20 mol % NdF_3 .

Experimental

Lithium fluoride (LiF), sodium fluoride (NaF), calcium fluoride (CaF_2), magnesium fluoride (MgF_2) and neodymium fluoride (NdF_3) were the analytical grade chemicals utilized to make the samples. Prior to usage, the compounds were dried in a vacuum furnace at 430 °C. To maintain the chemicals and make the samples, a glovebox (JACOMEX, France) with an argon atmosphere (SIAD Slovakia, purity 99.999%) was used (humidity under 5 ppm and oxygen content less than 2 ppm).

The experimental conductivity cell (Fig. 1) was composed of a pyrolytic boron nitride (pBN) tube (Boralloy, Momentive, USA) of 4 mm ID and 100-mm length. The graphite crucible (9) served as the counter electrode, while the platinum–rhodium alloy rod (1 mm OD) (1) put in place inside the pBN tube (7) served as the primary electrode. Approximately 60 g of the salt mixture (8) was contained

Fig. 1 Sketch of the experimental setup: (1) Pt–Rh electrode, (2) alumina-based radiation sheets, (3) heating elements, (4) boron nitride body of the electrode attachment, (5) Pt/Pt10Rh thermocouple, (6) stainless steel connector of the graphite crucible, (7) pyrolytic boron nitride tube, (8) melt, (9) graphite crucible, (10) alumina tube of the furnace and (11) flange of the furnace



in a crucible that was set up in a vertical laboratory furnace with an argon environment. Pure argon was heated in a copper mesh vessel and dried by bubbling through H_2SO_4 to create a dry inert atmosphere in the furnace. Pt/Pt10Rh thermocouple (5) was used to gauge the furnace’s temperature.

An impedance gain-phase analyzer (National Instruments, operated by LabVIEW software) has been used to measure the cell’s impedance at a fixed frequency of 100 kHz with a disturbing signal amplitude of 10 mV. Within a LabVIEW software environment, the temperature of the furnace was controlled, and the impedance data acquisition was performed. The stimulating sinusoidal signals had a 10-mV amplitude. The real part of the impedance of each experimental sample was in this work continuously measured at a constant frequency of 100 kHz and a slowly decreasing furnace temperature (5 °C/min).

With pure molten NaCl (820 to 1050 °C), the constant of the conductivity cell, which reflects the cell’s dimensions, was determined (32.70 cm^{-1}). The Janz and Tomkins handbook [26] was used as a source for the values of the specific conductivity for molten NaCl. The cell resistance containing pure molten KCl was measured to complete the calibration. Then, using the cell constant concluded from NaCl, the specific conductivity of KCl was determined. The data taken from the Janz and Tomkins handbook [26] were compared to this value of the electrical conductivity of molten KCl. The accuracy was determined to be 3% or less. Experimental results showed that the cell constant was relatively stable, indicating a thermal and environmental inertness of

the conductivity cell’s materials. More details of the experimental method can be found elsewhere [27–31].

Results and discussion

The experimental data of the ionic electrical conductivity of all measured systems are depicted in Figs. 2, 3, 4, 5, 6, 7, 8 and 9. Figures 2, 4, 6 and 8 represent the data of ionic conductivity as a function of temperature (Fig. 2: $(LiF-CaF_2)_{eut-NdF_3}$; Fig. 4: $(LiF-NaF)_{eut-NdF_3}$; Fig. 6:

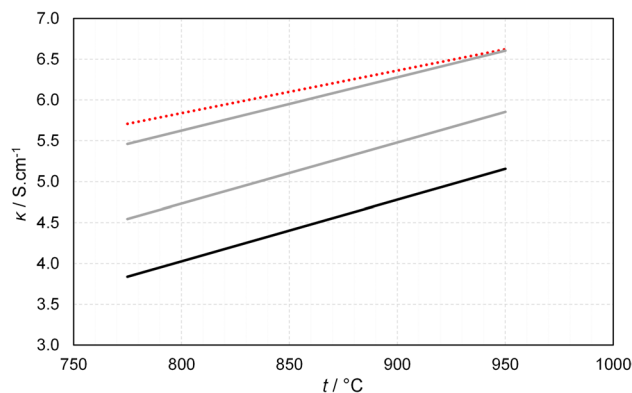


Fig. 2 The relationship between the ionic electrical conductivity of the molten system $(LiF-CaF_2)_{eut-NdF_3}$ and temperature. Black/grey full lines from bottom to up: 20, 15 and 5 mol % of NdF_3 . Red dotted line: 0 mol % NdF_3

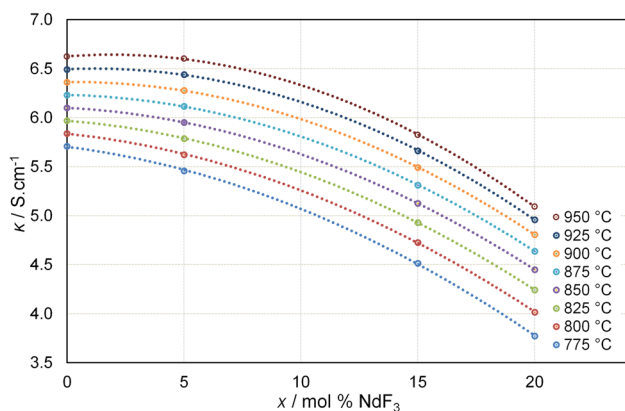


Fig. 3 The conductivity of the molten system (LiF–CaF₂)_{eut}–NdF₃ as a function of the concentration of NdF₃. Isotherms of the electrical conductivity are shown by dashed lines

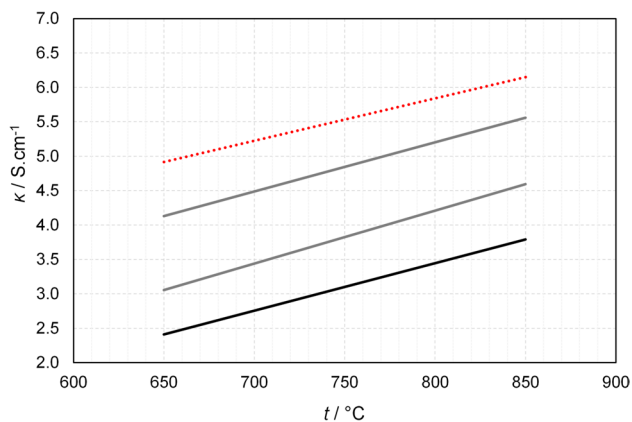


Fig. 4 The relationship between the ionic electrical conductivity of the molten system (LiF–NaF)_{eut}–NdF₃ and temperature. Black/grey full lines from bottom to top: 20, 10 and 5 mol % of NdF₃. Red dotted line: 0 mol % NdF₃

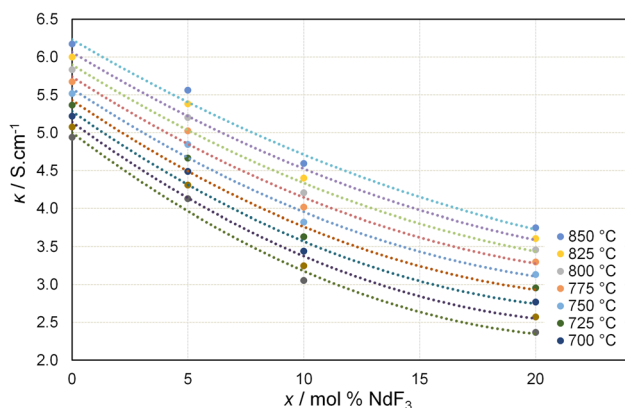


Fig. 5 The conductivity of the molten system (LiF–NaF)_{eut}–NdF₃ as a function of the concentration of NdF₃. Isotherms of the electrical conductivity are shown by dashed lines

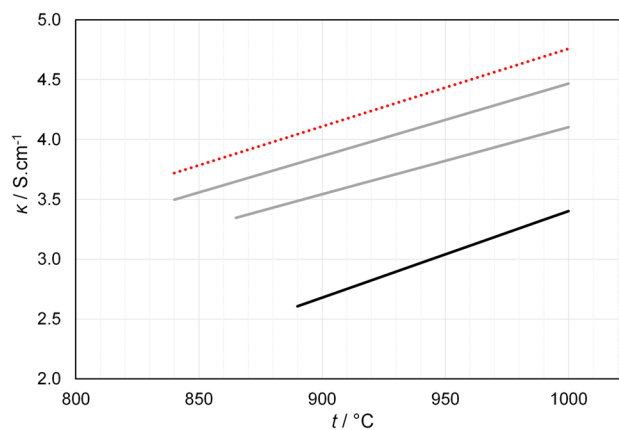


Fig. 6 The relationship between the ionic electrical conductivity of the molten system (NaF–CaF₂)_{eut}–NdF₃ and temperature. Black/grey full lines from bottom to up: 15, 10 and 5 mol % of NdF₃. Red dotted line: 0 mol % NdF₃

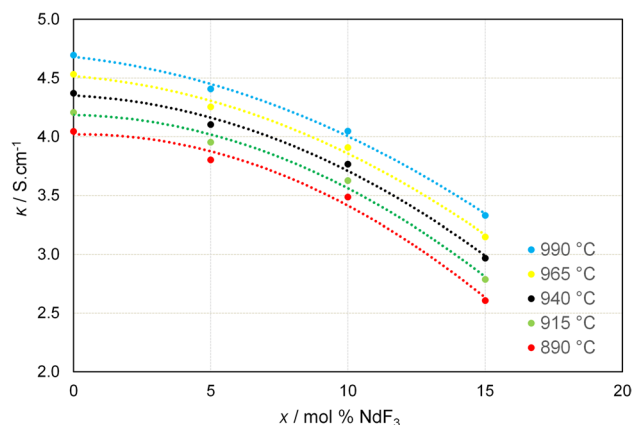


Fig. 7 The conductivity of the molten system (NaF–CaF₂)_{eut}–NdF₃ as a function of the concentration of NdF₃. Isotherms of the electrical conductivity are shown by dashed lines

(NaF–CaF₂)_{eut}–NdF₃ and Fig. 8: (LiF–MgF₂)_{eut}–NdF₃). Figures 3, 5, 7 and 9 show the isotherms of the ionic conductivity as a function of the NdF₃ concentration in the melt (Fig. 3: (LiF–CaF₂)_{eut}–NdF₃; Fig. 5: (LiF–NaF)_{eut}–NdF₃; Fig. 7: (NaF–CaF₂)_{eut}–NdF₃ and Fig. 9: (LiF–MgF₂)_{eut}–NdF₃). The experimentally determined results of the ionic electrical conductivity are described by the linear regression,

$$\kappa = a \cdot t - b \quad (1)$$

where κ (S.cm⁻¹) is the ionic conductivity of the melt, t (°C) is temperature and a (S.cm⁻¹.°C⁻¹) and b (S.cm⁻¹) are parameters of the regression. The parameters of the linear regression analysis of the experimental data of all measured molten systems are included in Tables 1, 2, 3 and 4.

The ionic conductivity of all investigated melts increases with the temperature and decreases with the

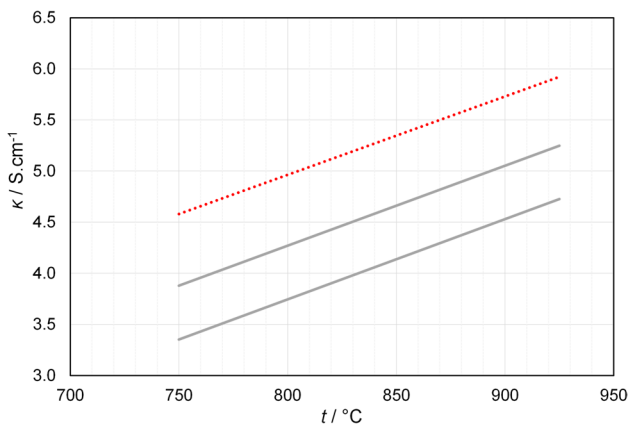


Fig. 8 The relationship between the ionic electrical conductivity of the molten system (LiF–MgF₂)_{eut}–NdF₃ and temperature. Gray full lines from bottom to up: 15 and 7 mol % of NdF₃. Red dotted line: 0 mol % NdF₃

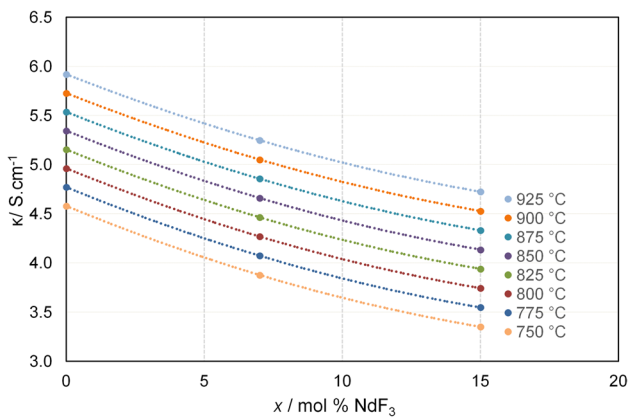


Fig. 9 The conductivity of the molten system (LiF–MgF₂)_{eut}–NdF₃ as a function of the concentration of NdF₃. Isotherms of the electrical conductivity are shown by dashed lines

Table 1 The data of the ionic electrical conductivity of the molten system (LiF–CaF₂)_{eut}–NdF₃ described by the Eq. 1. Temperature range: 775–950 °C

| x (mol % NdF ₃) | $a \cdot 10^3$ (S.cm ⁻¹ .°C ⁻¹) | $b \cdot 10^2$ (S.cm ⁻¹) |
|-------------------------------|--|--------------------------------------|
| 0 | 5.232 | – 165.34 |
| 5 | 6.535 | – 39.516 |
| 15 | 7.493 | 126.92 |
| 20 | 7.400 | 188.73 |

increasing concentration of NdF₃. The results of the ionic conductivity for the temperature 850 °C and for the NdF₃ concentrations 0, 10 and 15 mol %, respectively, can be compared as follows: the conductivity of

Table 2 The data of the ionic electrical conductivity of the molten system (LiF–NaF)_{eut}–NdF₃ described by the Eq. 1. Temperature range: 650–850 °C

| x (mol % NdF ₃) | $a \cdot 10^3$ (S.cm ⁻¹ .°C ⁻¹) | $b \cdot 10^2$ (S.cm ⁻¹) |
|-------------------------------|--|--------------------------------------|
| 0 | 6.288 | – 81.111 |
| 5 | 7.156 | 52.160 |
| 10 | 7.698 | 195.01 |
| 20 | 6.294 | 168.10 |

Table 3 The data of the ionic electrical conductivity of the molten system (NaF–CaF₂)_{eut}–NdF₃ described by the Eq. 1. Temperature range: 850–1000 °C

| x (mol % NdF ₃) | $a \cdot 10^3$ (S.cm ⁻¹ .°C ⁻¹) | $b \cdot 10^2$ (S.cm ⁻¹) |
|-------------------------------|--|--------------------------------------|
| 0 | 6.493 | 173.430 |
| 5 | 6.046 | 157.935 |
| 10 | 5.597 | 149.456 |
| 15 | 7.224 | 382.176 |

Table 4 The data of the ionic electrical conductivity of the molten system (LiF–MgF₂)_{eut}–NdF₃ described by the Eq. 1. Temperature range: 750–925 °C

| x (mol % NdF ₃) | $a \cdot 10^3$ (S.cm ⁻¹ .°C ⁻¹) | $b \cdot 10^2$ (S.cm ⁻¹) |
|-------------------------------|--|--------------------------------------|
| 0 | 7.655 | 116.043 |
| 7 | 7.833 | 199.644 |
| 15 | 7.854 | 253.937 |

the molten system (LiF–CaF₂)_{eut}–NdF₃ was determined to be 6.10, 5.95 and 5.10 S.cm⁻¹, the results for the system (LiF–NaF)_{eut}–NdF₃ were 6.16, 5.56 and 4.13 S.cm⁻¹, the results for (NaF–CaF₂)_{eut}–NdF₃ were 3.78, 3.56 and 2.32 S.cm⁻¹, and finally, the results for the system (LiF–MgF₂)_{eut}–NdF₃ were determined to be for the same temperature as 5.35, 4.79 and 4.14 S.cm⁻¹, respectively.

The various evolutions of the electrical conductivity drop upon the raising content of NdF₃ can be noted when comparing the isotherms of the electrical conductivity of our experimentally investigated systems. While it is clearly evident the rate of the conductivity drop in the system (LiF–CaF₂)_{eut}–NdF₃ as the amount of NdF₃ increases (Fig. 3), in the system (LiF–NaF)_{eut}–NdF₃, the conductivity decreases at lower concentrations linearly (0–15 mol %), and the rate of decreasing even slightly slows down in this system at higher concentrations of NdF₃ (15–20 mol %) (Fig. 5). A similar comparison can be said about the systems (NaF–CaF₂)_{eut}–NdF₃ and (LiF–MgF₂)_{eut}–NdF₃: an increased drop of the isothermal conductivity in the case

Table 5 The data of the ionic electrical conductivity of the molten system (LiF–CaF₂)_{eut}–NdF₃ as described by the Arrhenius Eq. (2). Temperature range: 775–950 °C

| <i>x</i> (mol % NdF ₃) | <i>A</i> ₀ (S.cm ⁻¹) | <i>E</i> _a (J.mol ⁻¹) |
|------------------------------------|---|--|
| 0 | 15.80 | 8881 |
| 5 | 20.65 | 11,607 |
| 15 | 26.95 | 15,541 |
| 20 | 29.84 | 17,872 |

Table 6 The data of the ionic electrical conductivity of the molten system (LiF–NaF)_{eut}–NdF₃ described by the Arrhenius Eq. (2). Temperature range: 650–850 °C

| <i>x</i> (mol % NdF ₃) | <i>A</i> ₀ (S.cm ⁻¹) | <i>E</i> _a (J.mol ⁻¹) |
|------------------------------------|---|--|
| 0 | 17.91 | 9990 |
| 5 | 21.94 | 12,835 |
| 10 | 31.99 | 18,097 |
| 20 | 27.95 | 18,691 |

Table 7 The data of the ionic electrical conductivity of the molten system (NaF–CaF₂)_{eut}–NdF₃ described by the Arrhenius Eq. (2). Temperature range: 850–1000 °C

| <i>x</i> (mol % NdF ₃) | <i>A</i> ₀ (S.cm ⁻¹) | <i>E</i> _a (J.mol ⁻¹) |
|------------------------------------|---|--|
| 0 | 26.205 | 18,069 |
| 5 | 24.434 | 17,993 |
| 10 | 23.081 | 18,283 |
| 15 | 55.639 | 29,577 |

of (NaF–CaF₂)_{eut}–NdF₃ and slow down in the conductivity decreasing in the case of (LiF–MgF₂)_{eut}–NdF₃.

The variation in temperature of the electrical conductivity can be expressed by the classic Arrhenius equation.

$$\kappa = A_0 \cdot e^{\frac{-E_a}{RT}} \quad (2)$$

*A*₀ (S.cm⁻¹) is the pre-exponential factor, *E*_a (J.mol⁻¹) is the activation energy, *R* (8.3145 J mol⁻¹.K⁻¹) is gas constant and *T* (K) is the absolute temperature. It is possible to replace Eq. 2 with the linear function ln(κ) = *f* (*T*⁻¹). Tables 3 and 4 present the Arrhenius plot's parameters (*A*₀ and *E*_a). It is evident that the NdF₃ content in the melt raises the activation energy of the ionic conductivity in all of the investigated systems. Tables. 5, 6, 7 and 8.

The electrical conductivity of melts and other coulombic liquids depends on the mass, size and energy of each interaction between the ions and their particular ionic environment. Ion size and interaction scale are variables

Table 8 The data of the ionic electrical conductivity of the molten system (LiF–MgF₂)_{eut}–NdF₃ described by the Arrhenius Eq. (2). Temperature range: 750–925 °C

| <i>x</i> (mol % NdF ₃) | <i>A</i> ₀ (S.cm ⁻¹) | <i>E</i> _a (J.mol ⁻¹) |
|------------------------------------|---|--|
| 0 | 26.52 | 14,951 |
| 7 | 30.65 | 17,585 |
| 15 | 34.20 | 19,729 |

Table 9 The data of the electrical conductivity (S.cm-1) measured at 850 °C

| | 0% mol NdF ₃ | 10% mol NdF ₃ | 15% mol NdF ₃ |
|--|-------------------------|--------------------------|--------------------------|
| (LiF–CaF ₂) _{eut} –NdF ₃ | 6.10 | 5.95 | 5.10 |
| (LiF–NaF) _{eut} –NdF ₃ | 6.16 | 5.56 | 4.13 |
| (NaF–CaF ₂) _{eut} –NdF ₃ | 3.78 | 3.56 | 2.32 |
| (LiF–MgF ₂) _{eut} –NdF ₃ | 5.35 | 4.79 | 4.14 |

that are coupled and represented the electrical conductivity's Arrhenius activation energy.

Given that the ionic radii of Li⁺ and Mg²⁺ cations are the smallest of those that could have been present in our investigated molten systems (size of radius: Mg²⁺ < Li⁺ < Ca²⁺ < Na⁺ < Na₂F⁺ < Nd³⁺), the higher electrical conductivity would have most likely been found in the molten systems based on MgF₂ and LiF. However, the Na⁺ cations are more movable in molten fluoride melts than Mg²⁺ cations, although some of the Na⁺ cations can be present in the molten fluorides also as bigger, less mobile dimers of Na₂F⁺. Table 9 summarizes the results of the electrical conductivity for 850 °C.

Looking at the electrical conductivity at 850 °C of pure eutectic systems LiF–CaF₂ (6.10 S.cm⁻¹) and LiF–NaF (6.16 S.cm⁻¹), one can see that they are similar compared to the eutectic systems LiF–MgF₂ (5.35 S.cm⁻¹) and NaF–CaF₂ (3.78 S.cm⁻¹). In the case of most conductive systems ((LiF–CaF₂)_{eut}–NdF₃ and (LiF–NaF)_{eut}–NdF₃), only at the higher concentrations of NdF₃, the electrical conductivity of the melts based on (LiF–CaF₂)_{eut} is more visibly higher than those based on (LiF–NaF)_{eut} (e.g., at 850 °C, it is 4.40 S.cm⁻¹ for the system ((LiF–CaF₂)_{eut}–20 mol % NdF₃, and 3.67 S.cm⁻¹ for the system (LiF–NaF)_{eut}–20 mol % NdF₃). It can be concluded that the best conductivity has a system based on LiF–CaF₂, and the worst has the system based on NaF–CaF₂ with a significant gap (ca 30% lower conductivity than the third most conductive system based on LiF–MgF₂ and ca 40% lower conductivity than the best conductive system based on LiF–CaF₂).

Conclusions

We measured and presented the electrical conductivity of the molten systems of $(\text{LiF}-\text{CaF}_2)_{\text{eut}}-\text{NdF}_3$, $(\text{LiF}-\text{NaF})_{\text{eut}}-\text{NdF}_3$, $(\text{NaF}-\text{CaF}_2)_{\text{eut}}-\text{NdF}_3$ and $(\text{LiF}-\text{MgF}_2)_{\text{eut}}-\text{NdF}_3$. The ionic conductivity of all investigated melts increased with the temperature and decreased with the increasing concentration of NdF_3 . It can be concluded that when heated to 850 °C the ionic electrical conductivity in the molten systems $(\text{LiF}-\text{CaF}_2)_{\text{eut}}-\text{NdF}_3$ and $(\text{LiF}-\text{NaF})_{\text{eut}}-\text{NdF}_3$ is approximately similar ($6.10 \text{ S}\cdot\text{cm}^{-1}$ and $6.16 \text{ S}\cdot\text{cm}^{-1}$, respectively for 0 mol % of NdF_3) compared to the conductivity of the systems $(\text{NaF}-\text{CaF}_2)_{\text{eut}}-\text{NdF}_3$ and $(\text{LiF}-\text{MgF}_2)_{\text{eut}}-\text{NdF}_3$ ($3.78 \text{ S}\cdot\text{cm}^{-1}$ and $5.35 \text{ S}\cdot\text{cm}^{-1}$, respectively for 0 mol % of NdF_3). The further results of the ionic conductivity for the temperature 850 °C can be for the concentrations of 10 and 15 mol % of NdF_3 stated, respectively, as follows: the conductivity of the molten system of $(\text{LiF}-\text{CaF}_2)_{\text{eut}}-\text{NdF}_3$ was determined to be 5.95 and $5.10 \text{ S}\cdot\text{cm}^{-1}$, the results for the system $(\text{LiF}-\text{NaF})_{\text{eut}}-\text{NdF}_3$ were 5.56 and $4.13 \text{ S}\cdot\text{cm}^{-1}$, the results for the system $(\text{NaF}-\text{CaF}_2)_{\text{eut}}-\text{NdF}_3$ were 3.56 and $2.32 \text{ S}\cdot\text{cm}^{-1}$. Finally, the results for the system $(\text{LiF}-\text{MgF}_2)_{\text{eut}}-\text{NdF}_3$ were determined to be as 4.79 and $4.14 \text{ S}\cdot\text{cm}^{-1}$.

When the amount of NdF_3 in both systems increased, a distinct isothermal drop in electrical conductivity was seen. While it is clear that the conductivity decreases more quickly in the systems based on $\text{LiF}-\text{CaF}_2$ and $\text{NaF}-\text{CaF}_2$ as the amount of NdF_3 increases, this is not the case in the systems based on $\text{LiF}-\text{NaF}$ and $\text{LiF}-\text{MgF}_2$, where this drop of the conductivity slowly decreases with the increasing concentration of NdF_3 . The rise in ion size and ion mass can be behind the decrease of the electrical conductivity with increasing concentration of NdF_3 . Additionally, it is also manifested in an increase in the activation energy of electrical conductivity. The decrease in electrical conductivity caused by the addition of NdF_3 could be due to the development of larger complex anions with a higher propensity to form longer chains linked via fluorine anions.

Author contribution Conceptualization: [Michal Korenko], [Dhiya Krishnan], [Aydar Rakhmatullin], [Lóránt Szatmáry]; Methodology: [Dhiya Krishnan], [Marta Ambrová], [Aydar Rakhmatullin], [František Šimko]; Formal analysis and investigation: [Michal Korenko], [Dhiya Krishnan]; Writing—original draft preparation: [Michal Korenko], [Michal Korenko]; Writing—review and editing: [Michal Korenko], [Dhiya Krishnan], [František Šimko], [Marta Ambrová], [Lóránt Szatmáry], [Aydar Rakhmatullin]; Funding acquisition: [František Šimko], [Michal Korenko]; Resources: [František Šimko]; Supervision: [Michal Korenko].

Funding Open access funding provided by The Ministry of Education, Science, Research and Sport of the Slovak Republic in cooperation with Centre for Scientific and Technical Information of the Slovak Republic This study was financially supported by the Slovak grant

agencies APVV–19–0270 and VEGA 2/0046/22. The work was performed within the ITMS project (with code 313021T081) supported by Research & Innovation Operational Programme funded by the ERDF.

Data availability This is not applicable.

Declarations

Ethical approval This is not applicable.

Competing interests The authors declare no competing interests.

Open Access This article is licensed under a Creative Commons Attribution 4.0 International License, which permits use, sharing, adaptation, distribution and reproduction in any medium or format, as long as you give appropriate credit to the original author(s) and the source, provide a link to the Creative Commons licence, and indicate if changes were made. The images or other third party material in this article are included in the article's Creative Commons licence, unless indicated otherwise in a credit line to the material. If material is not included in the article's Creative Commons licence and your intended use is not permitted by statutory regulation or exceeds the permitted use, you will need to obtain permission directly from the copyright holder. To view a copy of this licence, visit <http://creativecommons.org/licenses/by/4.0/>.

References

- Grjotheim K, Kvande H, Qingfeng L, Zhuxian Q (1998) Metal production by molten salt electrolysis: especially aluminium and magnesium. China University of Mining and Technology Press, Xuzhou
- Thonstad J, Fellner P, Haarberg GM, Híveš J, Kvande H (2001) *Å Sterten, Aluminium electrolysis*. Aluminium Verlag, Duesseldorf
- M Gaune-Escard, GM Haarberg (ed.), (2014) *Molten salts chemistry and technology*, John Wiley & Sons
- Lovering GD (ed) (1982) *Molten salt technology*. Plenum Press, New York
- A Misra, J Whittenberger (1987) *Fluoride salts and container materials for thermal energy storage applications in the temperature range 973 to 1400 K*. National Aeronautics and Space Administration NASA Lewis Technical Memorandum 89913 AIAA–87–9226
- D Williams (2006) *Assessment of candidate molten salt coolants for the NNGP/NHI heat-transfer loop Oak Ridge National Laboratory, RONL/TM-2006/69*
- Forsberg CW, Peterson P, Zhao H (2007) *High-temperature liquid-fluoride-salt closed-Brayton-cycle solar power towers*. *J Sol Energy Eng* 129:141–146
- O Beneš, RP Souček (2020) *Molten salt reactor fuels*. R. G. Bautista, M. M. Wong, M.H.A. Piro, (ed.), *Advances in nuclear fuel chemistry*, Woodhead Publishing Series in Energy, Elsevier, Amsterdam 249–271
- Roper R, Harkema M, Sabharwall P, Riddle C, Chisholm B, Day B, Marotta P (2022) *Molten salt for advanced energy applications: a review*. *Ann Nucl Energy* 169:108924
- LeBlanc D (2010) *Molten salt reactors: a new beginning for an old idea*. *Nucl Eng Des* 240:1644–1656
- Boullon R, Jaboulay JCh, Aubert J (2021) *Molten salt breeding blanket: investigations and proposals of pre-conceptual design options for testing in DEMO*. *Fusion Eng Des* 171:112707
- Nuttin A, Heuer D, Billebaud A, Brissot R, Le Brun C, Liatard E, Loiseaux JM, Mathieu L, Meplan O, Merle-Lucotte E, Nifenecker

- H, Perdu F, David S (2005) Potential of thorium molten salt reactors: detailed calculations and concept evolution with a view to large scale energy production. *Prog Nucl Energy* 46:77–99
13. Daněk V (2006) *Physico-chemical analysis of molten electrolytes*. Elsevier, Amsterdam
 14. Ray HS (2006) *Introduction to melts, molten salts, slags and glasses*. Allied Publishers, New Delhi
 15. Mlynáriková J, Boča M, Gurišová V, Macková I, Netriová Z (2016) Thermal analysis and volume properties of the systems $(\text{LiF}-\text{CaF}_2)_{\text{eut.}}-\text{LnF}_3$ ($\text{Ln} = \text{Sm}, \text{Gd}, \text{and Nd}$) up to 1273 K. *J Therm Anal Calorim* 124:973–987
 16. Sokol'skii VE, Roika AS, Davidenko AO, Faidyuk NV, Savchuk RN (2013) Xray diffraction study of the $\text{NaF}-\text{LiF}-\text{NdF}_3$ eutectic in the liquid and solid states *Inorg. Mater* 49:844–851
 17. Faidyuk NV, Savchuk RN, Omeľchuk AA (2014) Physicochemical properties of nonvariant composition of ternary $\text{NaF}-\text{LiF}-\text{LnF}_3$ systems ($\text{Ln} = \text{La}, \text{Nd}$). *ECS Trans* 64:197–205
 18. Fedorov PP (1999) Systems of alkali and rare earth metal fluorides. *Russ J Inorg Chem* 44:1703–1727
 19. Thoma RE, Insley H, Herbert GM (1966) The sodium fluoride–lanthanide trifluoride systems. *Inorg Chem* 5:1222–1229
 20. Gaune-Escard M (2001) Analysis of the enthalpy of mixing data of binary and ternary rare earth ($\text{Nd}, \text{La}, \text{Y}, \text{Yb}$), Al–alkali metal–fluoride systems. *J Alloys Compd* 321:267–275
 21. Sobolev BP, Fedorov PP (1978) Phase diagrams of the $\text{CaF}_2-(\text{Y}, \text{Ln})\text{F}_3$ systems I. Experimental. *J Less-Common Met* 60:33–46
 22. Sobolev BP, Fedorov PP, Seiranyan KB, Tkachenko NL (1976) On the problem of polymorphism and fusion of lanthanide trifluorides. II. Interaction of LnF_3 with MF_2 ($\text{M} = \text{calcium}, \text{strontium}, \text{barium}$). Change in structural type in the LnF_3 series, and thermal characteristics. *J Solid State Chem* 17:201–212
 23. Kubíková B, Mlynáriková J, Matselko O, Mikšíková E, Netriová Z, Vasková Z, Boča M (2022) Phase equilibria and volume properties of $(\text{LiF}-\text{MgF}_2)_{\text{eut.}}-\text{LnF}_3$ ($\text{Ln} = \text{Sm}, \text{Gd}, \text{Nd}$) Molten Systems. *J Mol Liq* 353:118694
 24. Kubíková B, Mlynáriková J, Wu Sh, Mikšíková E, Priščák J, Boča M, Korenko M (2020) Physicochemical investigation of the ternary $(\text{LiF} + \text{MgF}_2)_{\text{eut.}} + \text{LaF}_3$ molten system. *J Chem Eng Data* 65(10):4815–4826
 25. Zhu X, Sun Sh, Sun T, Liu Ch, Tu G, Zhang J (2020) Electrical conductivity of REF_3-LiF ($\text{RE} = \text{La}$ and Nd) molten salts. *J Rare Earths* 39:676–682
 26. Janz JG, Allen BC, Bansal NP, Murphy RM, RPT, (1979) Tomkins, Physical properties data compilations relevant to energy storage. II. Molten salts: data on single and multi-component salt systems, U.S. Government Printing Office, (NSRDS–NBS 61. Part II), Washington DC
 27. Korenko M, Priščák J, Šimko F (2013) Electrical conductivity of systems based on $\text{Na}_3\text{AlF}_6-\text{SiO}_2$ melts. *Chem Pap* 67:1350–1354
 28. Kim KB, Sadoway DE (1992) Electrical conductivity measurements of molten alkaline–earth fluorides. *J Electrochem Soc* 139:1027–1033
 29. X Wang, RD Peterson, AT Tabereaux (1992) Electrical conductivity of cryolitic melts, in: E.R. Cutshall (Ed.), *Proceedings of the 121st TMS Annual Meeting, The Minerals, Metals & Materials Society, San Diego* 481–488
 30. Fellner JP, Kobbeltvedt O, Sterten Å, Thonstad J (1993) electrical conductivity of molten cryolite–based binary mixtures obtained with a tube–type cell made of pyrolytic boron nitride. *Electrochim Acta* 38:589–592
 31. Híveš J, Thonstad J, Sterten Å, Fellner P (1996) Electrical conductivity of molten cryolite–based mixtures obtained with a tube–type cell made of pyrolytic boron nitride. *Metall Mat Trans B* 27:255–261

Publisher's Note Springer Nature remains neutral with regard to jurisdictional claims in published maps and institutional affiliations.